

## Accepted Manuscript

Gear misalignment diagnosis using statistical features of vibration and airborne sound spectrums

Muhammad Ali Khan, Muhammad Atayyab Shahid, Syed Adil Ahmed, Sohaib Zia Khan, Kamran Ahmed Khan, Syed Asad Ali, Muhammad Tariq

PII: S0263-2241(19)30532-9  
DOI: <https://doi.org/10.1016/j.measurement.2019.05.088>  
Reference: MEASUR 6697

To appear in: *Measurement*

Received Date: 18 April 2018  
Revised Date: 11 March 2019  
Accepted Date: 25 May 2019



Please cite this article as: M.A. Khan, M.A. Shahid, S.A. Ahmed, S.Z. Khan, K.A. Khan, S.A. Ali, M. Tariq, Gear misalignment diagnosis using statistical features of vibration and airborne sound spectrums, *Measurement* (2019), doi: <https://doi.org/10.1016/j.measurement.2019.05.088>

This is a PDF file of an unedited manuscript that has been accepted for publication. As a service to our customers we are providing this early version of the manuscript. The manuscript will undergo copyediting, typesetting, and review of the resulting proof before it is published in its final form. Please note that during the production process errors may be discovered which could affect the content, and all legal disclaimers that apply to the journal pertain.

# Title: Gear misalignment diagnosis using statistical features of vibration and airborne sound spectrums

## Corresponding Author:

1. Muhammad Ali Khan

School of Aerospace, Transport and Manufacturing, Cranfield University, UK,  
[muhammad.a.khan@cranfield.ac.uk](mailto:muhammad.a.khan@cranfield.ac.uk) , Telephone: +44 (0) 1234 754788

## Co-Authors:

2. Muhammad Atayyab Shahid

Department of Engineering Sciences, Pakistan Navy Engineering College, National University of Sciences and Technology, Karachi, Pakistan, [atayyabshahid@gmail.com](mailto:atayyabshahid@gmail.com)

3. Syed Adil Ahmed

Department of Engineering Sciences, Pakistan Navy Engineering College, National University of Sciences and Technology, Karachi, Pakistan, [adilahmed\\_95@yahoo.com](mailto:adilahmed_95@yahoo.com)

4. Sohaib Zia Khan

Department of Mechanical Engineering, Islamic University of Madinah, Madinah, KSA  
[szkhan@iu.edu.sa](mailto:szkhan@iu.edu.sa)

5. Kamran Ahmed Khan

Department of Aerospace Engineering, Khalifa University, Abu Dhabi, United Arab Emirates  
[kamran.khan@kustar.ac.ae](mailto:kamran.khan@kustar.ac.ae)

6. Syed Asad Ali

Department of Engineering Sciences, Pakistan Navy Engineering College, National University of Sciences and Technology, Karachi, Pakistan, [asad1995ali@hotmail.com](mailto:asad1995ali@hotmail.com)

7. Muhammad Tariq

Department of Engineering Sciences, Pakistan Navy Engineering College, National University of Sciences and Technology, Karachi, Pakistan, [muhammad.tariq@pnec.nust.edu.pk](mailto:muhammad.tariq@pnec.nust.edu.pk)

## Abstract:

Failure in gears, transmission shafts and drivetrains is very critical in machineries such as aircrafts and helicopters. Real time condition monitoring of these components, using predictive maintenance techniques is hence a proactive task. For effective power transmission and maximum service life, gears are required to remain in perfect alignment but this task is just beyond the bounds of possibility. These components are flexible, thus even if perfect alignment is achieved, random dynamic forces can cause shafts to bend causing gear misalignments. This paper investigates the change in energy levels and statistical parameters including Kurtosis and Skewness of gear mesh vibration and airborne sound signals when subjected to lateral and angular shaft misalignments. Novel regression models are proposed after validation that can be used to predict the degree and type of shaft misalignment, provided the relative change in signal RMS from an aligned condition to any misaligned condition is known.

**Keywords:** Gearbox, Misalignment, Vibration, Acoustic, Prediction, Statistics

## 1. Introduction

Gearboxes are widely used in automobiles, aircrafts, helicopters and nuclear power plants to transmit motion and vary speed and torque. Failure of a gear in these applications can lead tragic incidents and can have serious consequences on human lives. In 1999, 28 out of 192 failure of helicopters were primarily due to gearbox failure [1]. In 2011, a Puma helicopter crashed in the North Sea because of a gearbox failure due to a faulty maintenance error [2]. After these incidents, the employment of the Health Usage and Monitoring Systems (HUMS) was recommended on helicopters for predicting impending component failure for maintenance at an early stage and warning pilots of imminent

degradation in gearboxes and drivetrain [3]. Vibration and noise based health monitoring techniques are considered viable for many rotating and reciprocating machines especially gearboxes [4-7]. Using these techniques along with deployment of advanced sensors has now become conventional on all helicopters and for other machines. The technologies have now matured enough claiming a number of successes with respect to accident prevention. The HUMS at present is around 70% effective in evaluating the airworthiness of any aerospace structure [8]. The improvement in setting appropriate thresholds for the gearbox condition indicators (CIs) can also take place through investigation of gear mesh misalignments since the vibration and noise study on the mentioned misalignments is not widely studied in the literature.

Earlier studies on the dynamic behavior of gear pairs investigated the effect of increasing speeds on gear teeth loads and the corresponding reduction in service life [9]. Tharmakulasingham investigated the effect of transmission errors (TE) on the dynamic behavior of the spur gears [10]. It was suggested that the tooth profile errors and variation in the torsional mesh stiffness cause generation of abnormal gear vibration and noise. Other sources of the abnormal dynamic behavior of gears are characterized under axial forces from bearings, eccentricity errors in gear shafts and pitch errors. Åkerblom [11] stated the contact deformations (due to Hertz contact stresses, teeth bending, run-out errors, gear blank deflections, shaft and bearing deflections) as another source of abnormal gear vibration. The transmission errors were classified into 4 types, namely, 1) manufacturing transmission errors due to errors in tooth geometry, 2) static transmission error that occurs at low load conditions as teeth deform elastically, 3) kinetic transmission error that occurs due to asperities contact on tooth surface like surface roughness and ruggedness, and, 4) dynamic transmission error that could occur due to dynamic forces. A new approach proposed the tooth contact analysis for geared systems and investigated the effect of loads on TE [12]. More et al. investigated the effect of TE, misalignment and manufacturing errors on the shuttling force excitations and overall noise generated in a helical gearbox using a load distribution program and Finite Element Analysis (FEA). The contribution of shuttling moment and TE in generation of vibration signals was also discussed in later research [13]. Zhan et al. developed a novel method by integrating FEA and numerical algorithms for evaluating the time varying torsional mesh stiffness of gears [14]. The simulation of gearbox components was also used to identify the causes of gear failures including TE, macro and micro geometrical errors, material homogeneity errors and other possible causes of gear noise to optimize and improve gearbox life [15]. Zhang et al. incorporated the unavoidable meshing errors in their study on the gear tooth modification (GTM) and provide an improved shape for the gear dynamic performance [16]. The effects of constant and fluctuating loads and the shaft speed on the helical gear dynamic response were used to establish a direct relation between shaft speed and its alignment [17]. With rising demand for electronic vehicles (EV), the dynamic requirements for the gear systems will change as it will be possible to run gears at higher speeds on electric motors compared to internal combustion (IC) engines. Harris et al. simulated gear misalignments, contact patches, TE, system deflections and the complete drivetrain of an EV [18]. They also compared conventional noise, vibration and harshness to understand sources of noise in an EV transmission. The Monte Carlo simulations were also used to evaluate minimum backlash in gear dynamics studies [19]. These simulations were helpful to analyze the gear responses under misalignments, face width variation, center distance variation, lead, run-out and pitch variations.

The past research efforts related to misaligned gears mostly used the finite element analysis for the stress evaluation under different misalignments and load conditions. Hani [20] in his work evaluated the effect of shaft misalignments on the stress distribution of the spur gears. He showed using FEA that the stresses distribution and its concentration on tooth were directly proportional to the misalignment angle. Similar work was reported on the effects of linear and angular misalignments of a spur gear pair [21]. The research work evaluated the effects of misalignments on the mesh stiffness variation, the load sharing ratios and the mesh forces on teeth. Prabhakaran [22] performed FEA for the stress evaluation of the spur gears subjected to the yaw misalignments at 1 and 2 degrees. The evaluation of stresses in axial misalignment condition was also reported in a later research [23]. These studies helped to

determine the strength of gears under misalignment but not expressing the details about the gear dynamic responses.

The experimentation and numerical based research on vibrations of misaligned gears is relatively new; and as per authors' knowledge the first and only paper yet on the problem was published in 2012 [24]. The work reported the changes in the vibration signatures due to the axial and the radial misalignments in the gear meshing region, using a limited set of experimentations for each type. It also highlighted the need for further experimentations to develop stronger correlations. Recently, the effects of the tooth tip corner contact and the shaft misalignments with high contact ratio gears were also analyzed using FEA [25]. They used different flank sizes and compared tooth sharing loads for each case.

The gears should be in perfect mesh alignment for an efficient power transmission. This perfect teeth alignment provides a uniform load distribution on the teeth which can maximize the gear service life and hence reduce the probability of a premature failure. The vibration and the noise characteristics in gear meshing under different shaft misalignments is not comprehensively discussed in the available literature. Therefore, the prime objective of this paper is to empirically investigate these characteristics and analyze them with the help of the condition indicators like RMS energy, Kurtosis and Skewness. This paper highlights the change in energy levels of regular components of a gear mesh (Fast Fourier Transform) FFT when subjected to a change in the meshing areas due to degrees of axial, radial, yaw and pitch shaft misalignments. A torsional loaded spur gear test rig was used in experiments with vibration and airborne sound sensors. Novel regression models were also proposed after validation. These models were used to predict the degree and type of the shaft misalignment if the relative change in signal RMS from an aligned condition to any misaligned condition was available.

## 2. Gear Misalignments and Condition Indicators

Gears are designed for a long operational life and with a high factor of safety but this can be compromised if the lubrication quality falls, shaft bearings wear out, shaft loses eccentricity or shaft bends/deforms resulting in teeth to lose the perfect alignment condition displayed in Fig. 1 (a). Teeth misalignments cause gears to run under increased loads and as a result contact stresses rise. Two types of lateral and angular gear shaft misalignments were experimentally tested and analyzed in this paper as shown in Fig.1 and described below:

### 2.1 Lateral Misalignment:

2.1.3 Radial Misalignment: Gears are subjected to radial misalignment when gear teeth are brought away from each other by increasing the center-to-center distance while the shafts remain parallel as shown in Fig. 1 (b). It reduces the contact area of the teeth under mesh and hence ultimately reduces the teeth meshing stiffness (the resistance of teeth to deformation when in the meshing region due to the hertz contact stresses). The backlash and tooth bending also increases as the meshing contact region moves nearer to the addendum or tooth tip. Furthermore, the contact ratio also reduces due to lesser asperities in contact and hence reduces the gear noise.

2.1.4 Axial Misalignment: When subjected to axial misalignment, the gears center-to-center distance remains unchanged, but one gear is advanced along its axis forward, so that contact is lost along some of its face width as shown in Fig. 1 (c). Although the contact ratio and backlash remains same, the contact area decreases and due to increased contact stresses and deformation, there is a reduction in meshing stiffness.

### 2.2 Angular Misalignment:

2.2.1 Yaw Misalignment: In this misalignment, the gear shafts are positioned non-parallel and moved at an angle on the horizontal plane as shown in Fig. 1 (d). Gears are then subjected to an increase or decrease in the contact area depending on whether the pinion shaft is displaced towards or away from the gear shaft at a horizontal angle. The contact ratio changes as the misalignment angle is varied. If the pinion shaft is displaced towards the gear at a horizontal angle, the pinion teeth intrude further into gear, reducing the gear clearance from optimal value. Hence, the asperities in contact should increase, causing

more gear noise. While if the pinion is displaced away from the gear, gear backlash increases, the contact ratio and the asperities in contact decreases and resulting a low noise.

**2.2.2. Pitch Misalignment:** Gears can be subjected to pitch misalignment, when the pinion and the gear shafts are misaligned by introducing an angle in the vertical plane as shown in Fig. 1 (e). As the pinion shaft is displaced at a vertical angle, its teeth are tilted and hence more edge region comes in contact in meshing region compared to the rest of the face width. This causes contact to be at a point rather than on a line (as in perfect alignment case) which can increase the deformation and reduce the mesh stiffness. Pitch misalignment causes more edge wear on flank and provides reduced cushioning effect (i.e. Gears come into impact and separation on the flank edge while meshing). According to the FEA analysis performed in previous studies [24], pitch misalignment causes most rise in contact stresses as compared to the others.

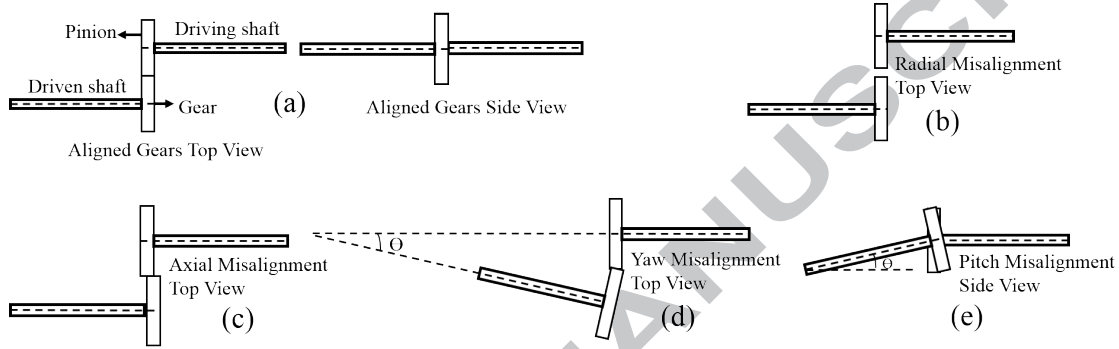


Fig. 1 Misalignment Cases

Condition indicators (CI) [26-29] were normally employed on the vibration and the noise signals to evaluate the health/condition of a gearbox. Gearboxes were subjected to the degrees of tooth cut/breakage and improper chamfering [30] in previous studies and mainly crack growth in gear tooth or rim was studied by using the vibration and the noise signals and their respective CIs [31-36]. However, there will be a dominant change in the vibration and the noise signatures if the gears are subjected to the above mentioned misalignments. These changes in the mentioned signature are not widely studied in published literature and hence is the focus of this presented research work. The primary CI which is used in this work, is the Root Mean Square (RMS) energy analysis. Kurtosis and Skewness are also used to validate the trend in RMS. In RMS Energy Analysis, the RMS function [37-40] is based on the energy content of vibration or noise signal in a cumulative manner as given in Equation 1.

$$RMS = \sqrt{\frac{1}{N} \sum_{i=1}^N s_i^2} \quad (1)$$

Where  $s_i$  is the  $i^{\text{th}}$  member in the dataset  $s$ , and  $N$  is the number of points in the dataset.

Kurtosis [26,29] defines the peakedness in the shape of the amplitude distribution of the signal as given in Equation 2. The Kurtosis is the fourth centralized moment of the signal and is normalized by the signal variance. The Kurtosis of a normal distribution is 3, values greater than 3 indicate a heavy tailed distribution while values lesser than 3 indicate light tailed distributions.

$$Kurtosis = \frac{N \cdot \sum_{i=1}^N (s_i - \bar{s})^4}{(\sum_{i=1}^N (s_i - \bar{s})^2)^2} \quad (2)$$

Skewness [26] indicates the symmetry of the amplitude distribution of the vibration and the airborne sound signal and is given in Equation 3. It is the third order moment in statistical analysis. Skewness of a normal distribution is zero, while negative skewness indicates data is shifted towards left and positive skewness indicates data is shifted to right side (i.e. the right tail is longer than left).

$$Skewness = \frac{N \cdot \sum_{i=1}^N (s_i - \bar{s})^3}{(\sum_{i=1}^N (s_i - \bar{s})^2)^{3/2}} \quad (3)$$

In Equation 2 and 3,  $N$  is the number of points in time domain of the signal,  $s_i$  is the  $i^{th}$  point in the signal and  $\bar{s}$  is the signal mean.

### 3. Experimental Procedure

A customized gear test rig was used to generate the vibration and the noise signatures under different misalignments. The rig has a provision for introducing degrees of different misalignments in its design. The experimental setup is shown in Fig. 2 (a). The driving motor which runs at 1500 rpm and 3 HP, was rested on an adjustable bed which was supported by horizontal and vertical screws. The movable bed accommodated the driving shaft which could be aligned by using the available vertical and horizontal screws. The gearbox contained a spur pinion and a gear. The driven gear was mounted on the shaft which was connected to a rotor based loading mechanism. The box of the loading mechanism was filled with viscous oil and hence on rotation offered resistance and loaded the gears torsionally. A constant oil level in the loading unit offered a torque load of 43.5 Nm and same was used in all experiments. The whole setup was also rested on a base table. The locations of accelerometer and microphone sensors are shown in Fig. 2 (a). The vertical plane and horizontal plane adjustment screws used for aligning and misaligning the driving shaft are shown in Fig. 2 (b) and (c).

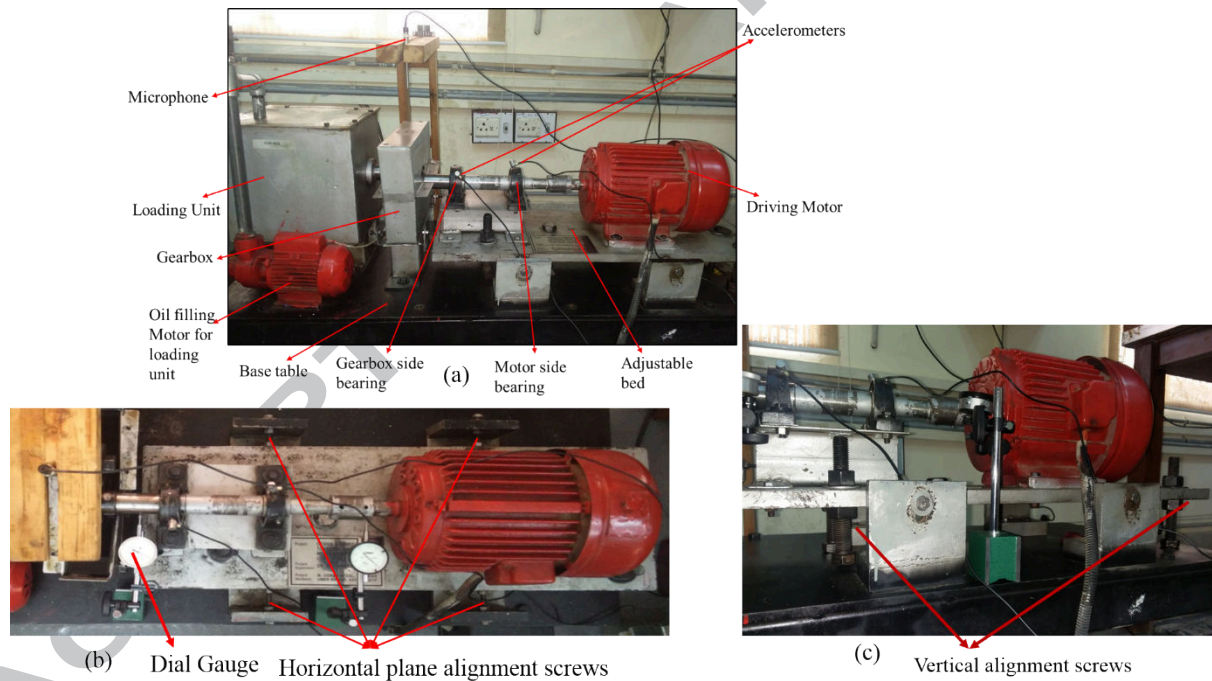


Fig. 2 Experimental Setup (a), showing horizontal plane (b) and vertical plane (c) adjustment screws

A set of analogue deflection dial gauges were also used for aligning the rig in horizontal plane as shown in Fig. 2 (b). A digital vernier caliper and a phone gyroscope were also employed for the vertical alignment as shown in Fig. 3. The same set of equipment was also used in introducing controlled misalignments during the tests. A schematic of positioning of the rig in the laboratory and the key sensor positions is given in Fig. 4.

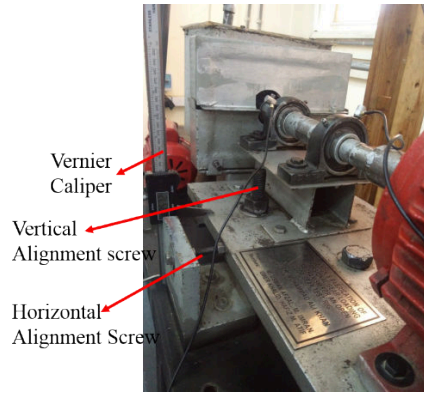


Fig. 3 Vernier Caliper for Vertical plane adjustment and for inducing pitch misalignment

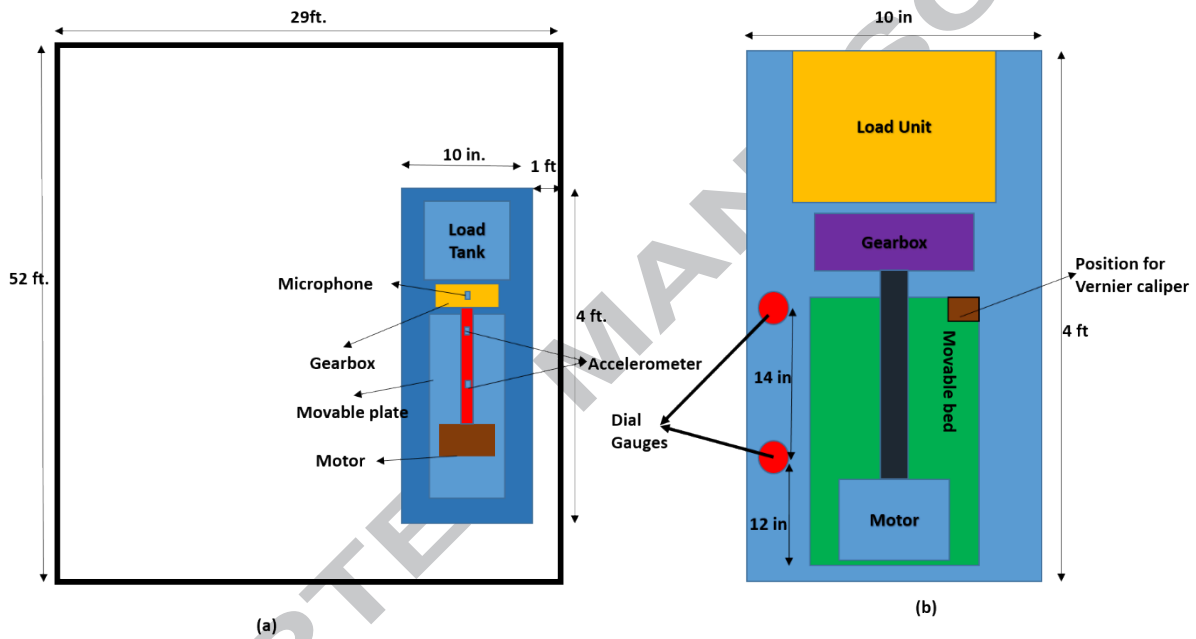


Fig. 4 Placement of the gear rig in the room (a), and key sensor and measurement positions on the gear rig (b)

Two Tenlee® single axis accelerometers were mounted on the motor and the gear side bearing for acquiring the vibration data. A GRAS® 40 PP microphone was placed directly above the gearbox for acquiring acoustic signals as shown in Fig. 2 (a). The sensors were connected to a DAQCard™ NI 9234 through NI cDAQ™ 9174 Chassis to a laptop. SignalExpress™ 2015 was used for signal acquisition and processing as shown in Fig. 5. The sensor characteristics for accelerometers and microphone is listed in Table 1.

Table 1 Sensor Properties

Sensor	Accelerometer	Microphone
Model No.	TL122A05	GRAS 40 PP
Sensitivity	4.81mV/g	50mV/Pa
Impedance	50 $\Omega$	50 $\Omega$
Frequency Range	Up to 12kHz	10Hz to 20 kHz
Temperature Range	-40 to 121 °C	-10 to 50 °C
Excitation Current	2-10 mA	2 to 20 mA

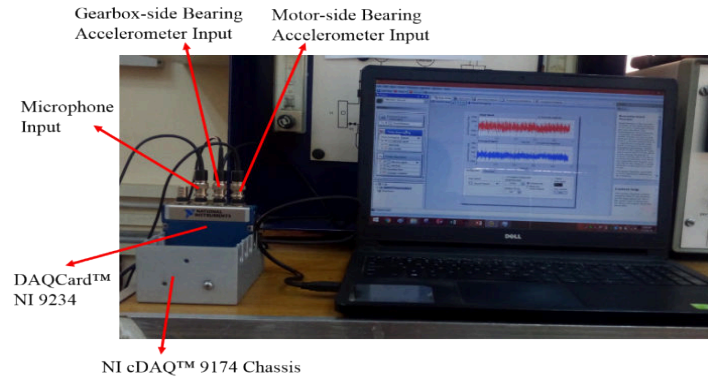


Fig. 5 Instrumentation and Signal processing setup

The pair of gears used in the experiments is shown in Fig. 6. The design parameters of the used gears are provided in Table 2. The material of the gears was AISI 4140 steel. The gear machining was performed on a CNC to achieve close tolerances; while CNC milling was carried out for the teeth grinding. The error tolerances of 5% were specified during manufacturing. Gears with close error tolerances were paired up for each misalignment case. Dimension errors of the gear pairs are given in Table 3.

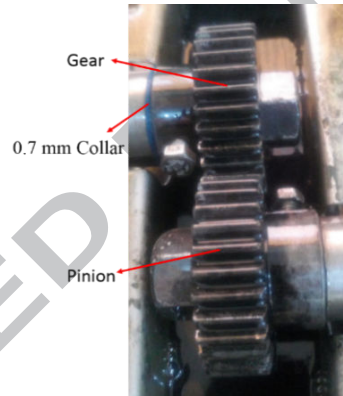


Fig. 6 Gearbox (with Axial misalignment spacer collar)

Table 2 Pinion and Gear design parameters

Gear Parameter	Design Value
Module	2.25
Number of teeth	31
Pitch Diameter	69.75 mm
Face width	21.2 mm

Table 3 Gear tolerance errors

Misalignment case	Gear No.	Pitch Diameter (mm)	Face-Width (mm)
Radial	Gear 1	72.65	22.02
	Gear 2	73.20	21.69
Axial	Gear 3	67.33	23.12
	Gear 4	68.21	23.59
Yaw	Gear 5	70.32	19.26
	Gear 6	70.07	19.53
Pitch	Gear 7	65.21	20.56
	Gear 8	66.03	21.07

#### 4. Methodology

For each type of misalignment, a new pair of spur gears was used. This was done in order to record just the effects of one type of misalignment on the gears. The zero alignment condition control reading was also performed each time for each gear pair when changing to a different misalignment type.

The perfect alignment in a gearbox is beyond the bounds of possibility and even close to perfect alignment is a very challenging milestone to achieve. A set of deflection dial gauges, Vernier caliper, and a gyroscope was used to achieve a zero misalignment with a 0.01 mm accuracy. These tools were used in aligning the movable bed which housed the driving pinion shaft. The zero-control position was marked on the rig using this equipment before any misalignment was done. This position was then used to induce other misalignments using the set of dial gauges, Vernier caliper and gyroscope. The experimental scheme is tabulated in Table 4.

Table 4 Experimental Scheme

Misalignment Case #	Gear Set	Misalignment Type	Misalignment Step	Signal Purpose
1	Pair 1	Radial	0.2 mm	For model development
2			0.3 mm	For RMS Validation
3			0.4 mm	For model development
4			0.6 mm	For model development
5			0.8 mm	For RMS Validation
6			1.0 mm	For model development
7	Pair 2	Yaw	+0.025 deg	For model development
8			+0.05 deg	For model development
9			+0.06 deg	For RMS Validation
10			+0.075 deg	For model development
11			+0.1 deg	For model development
12			-0.025 deg	For RMS Validation
13			-0.75 deg	For model development
14	Pair 3	Axial	1 collar = 0.7 mm	For model development
15			2 collar = 1.4 mm	For model development
16			3 collar = 2.1 mm	For RMS Validation
17			4 collar = 2.8 mm	For model development
18			5 collar = 3.5 mm	For RMS Validation

19			0.025 deg	For model development
20			0.05 deg	For model development
21			0.075 deg	For model development
22	Pair 4	Pitch	0.1 deg	For RMS Validation
23			0.15 deg	For RMS Validation
24			0.2 deg	For model development

For radial and yaw misalignments, the set of deflection dial gauges were used to take shaft displacement reading in radial and yaw misalignments cases. The horizontal plane alignment screws were used to move pinion shaft in these cases. For axial misalignment, collars of 0.7 mm thickness were used between the shaft and the gear to displace it on the axial axis as shown in Fig. 6.

The operational frequencies of the components of the gear rig as calculated for the mentioned experimental setup is shown in Table 5. The gear mesh frequency was of main interest in all the experiment. It was acquired at a sampling frequency of 3.5 kHz and the first two harmonics were recorded for analysis as used in the previous research [41]. Each raw signal was acquired by operating the gear rig for 4.2 minutes and the number of time averages was set at 250 on SignalExpress™. A high band pass filter with limit of 10 Hz was employed to remove the 0 Hz sensor DC offset peak [42] and low frequency noise, along with a Hanning window filter to minimize spectral leakage.

Table 5 Frequencies of the gear testing rig

Frequency	Value
Gear Rotational Frequency $F_{rg}$	25 Hz
Pinion Rotational Frequency $F_{rp}$	25 Hz
Gear Mesh Frequency $GMF$	775 Hz
Bearing Fundamental Train Frequency $FTF$	10.16 Hz
Ball Passing Frequency Outer (BPFO) Race	91.47 Hz
Ball Passing Frequency Inner (BPFI) Race	133.528 Hz
Ball Spin Frequency (BSF)	64.54 Hz

Each case listed in the experimental scheme was repeated three times which ensures the repeatability in the results. The time averaged and raw signals are shown in Fig. 7.

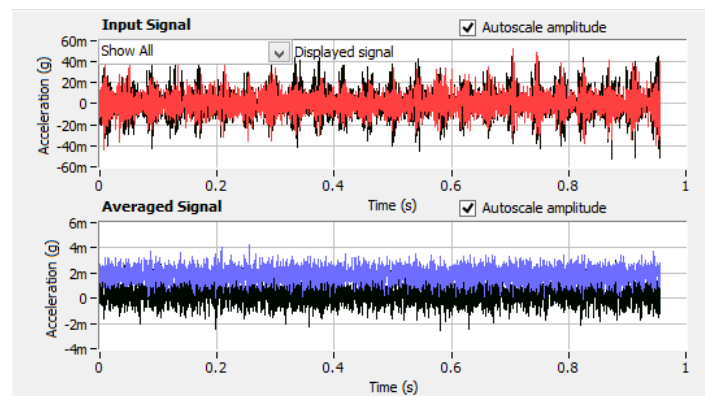


Fig. 7 Raw input (red) and time averaged (blue) signals in time domain

The FFT graphs for vibration and airborne signals of a control reading are illustrated in Figs. 8 and 9, respectively, with its regular components of interest marked. The frequency spectrum graphs were computed with RMS peak conversion in SignalExpress™. Same components from all cases of vibration and noise tests were used for further RMS analysis.

Kurtosis and Skewness analysis was carried out to support the trends observed in RMS. For this purpose, the raw signals were used to make amplitude histograms. The upper and lower bounds of the histogram was set equal to the maximum and minimum amplitude values of the time domain signal as shown in Fig 10. The bin size was calculated using the ceilings formula [43], given in Equation 4.

$$k = \frac{s_{max} - s_{min}}{h} \quad (4)$$

Where  $s_{max}$  is the maximum amplitude of the signal,  $s_{min}$  is the minimum amplitude and  $h$  is bin width calculated using Scotts Normal Reference Rule [44], given in Equation 5.

$$h = \frac{3.5\sigma}{\sqrt[3]{N}} \quad (5)$$

where  $\sigma$  is the standard deviation of the signal, and  $N$  is the number of samples in the signal. The number bins for all histograms was set equal to 40. The Kurtosis and Skewness of the histograms were calculated in Microsoft® Excel using the KURT and SKEW function respectively.

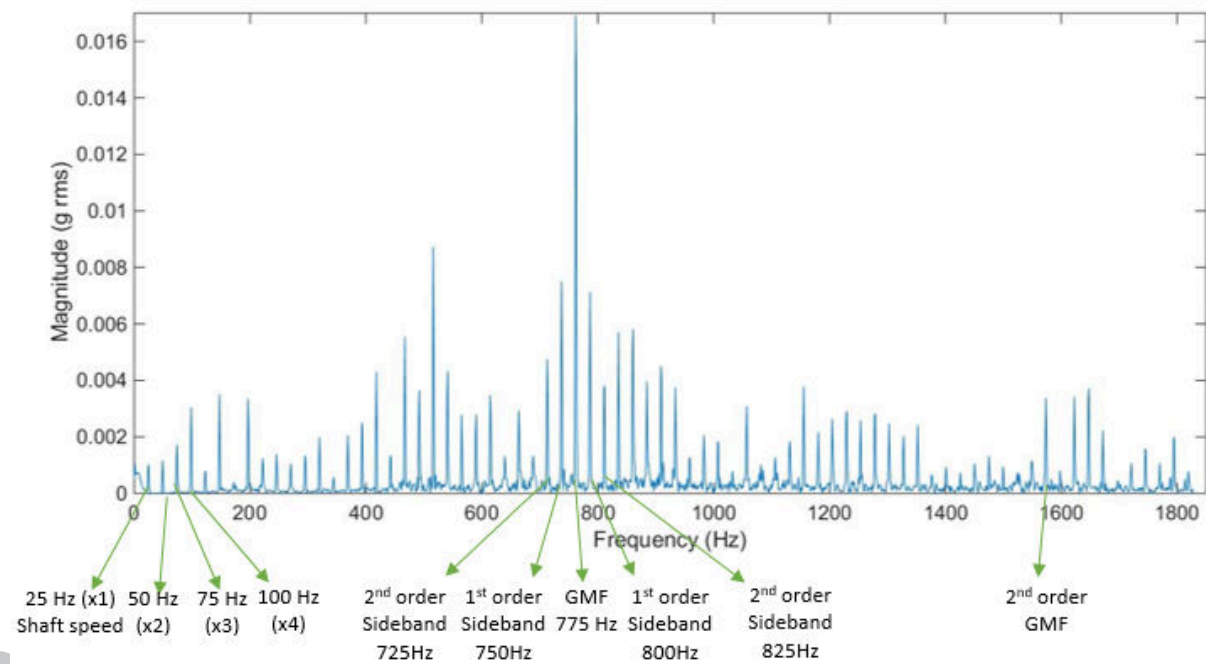


Fig. 8 Power Spectrum FFT graphs of a typical Vibration signal of the gearbox under test

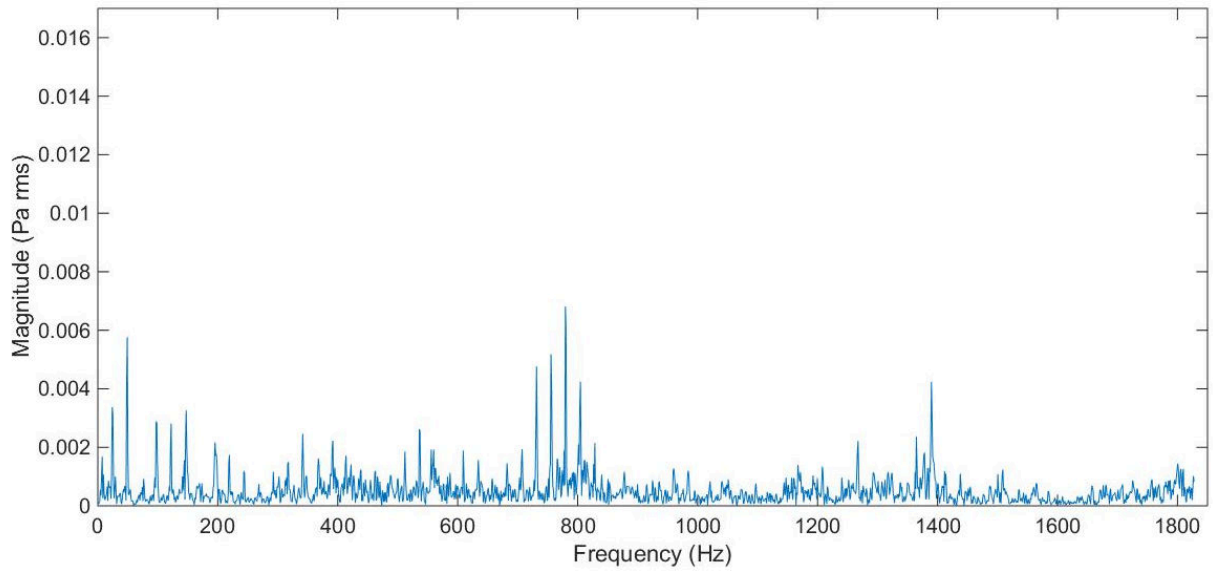


Fig. 9 A typical Airborne sound signal of the gearbox under test

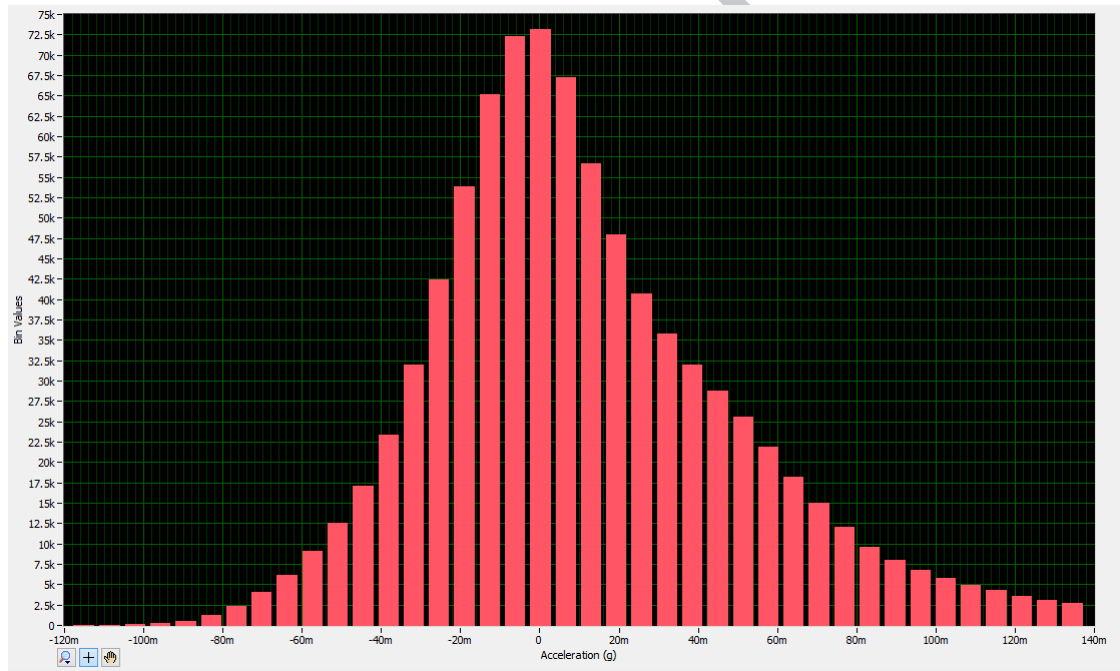


Fig. 10 Amplitude Histogram for a typical Vibration Signal of the gearbox in SignalExpress™

The baseline spectrum for gear pairs used in all misalignment cases is given in Fig. 11. The variation in these spectrums is due to slight differences in gear geometry because of manufacturing errors. Partially the variations are also due to the fact that exactly the same aligned condition is not possible to achieve every time and there may be slight dissimilarity in while aligning gears each time.

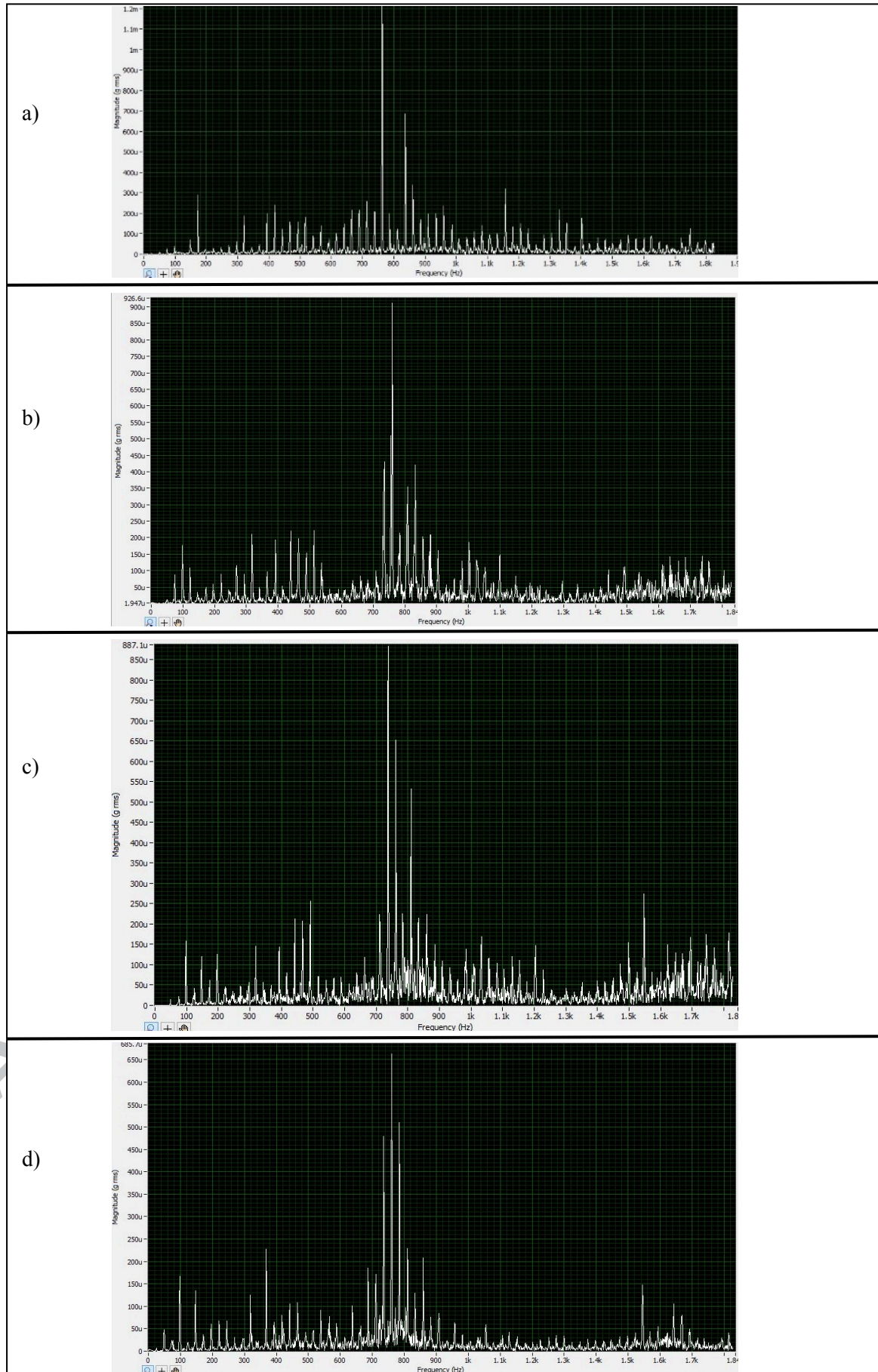


Fig. 11 Baseline vibration signals for a) radial b) axial c) yaw & d) pitch misalignment

## 5. Results

The RMS analysis of vibration and air-borne sound signals of the gearbox was carried out in SignalExpress™. In the past research [41–42, 45], the effect of misalignments in the rotating shafts was reflected in the FFT spectrum specially affecting the shaft speed harmonics peaks and the gear mesh frequency region. It was believed that the increasing shaft misalignments tend to increase the RMS energy of first few harmonics of the shaft speed frequency and also caused the leakage of the main gear mesh frequency energy into its sidebands. It was mentioned in the literature [46] that the misalignments in the shafts affect the 1X, 2X and 3X peaks of the shaft speeds on the FFT spectrum. But the available literature is still unable to mention which type of misalignment tends to affect a specific shaft speed harmonic the most. Therefore, the RMS peak values of the regular components in the frequency spectrum were measured for each misalignment case alongside with the total RMS values. The RMS values were fitted by using the MATLAB® Curve Fitting Toolbox™ and were plotted for each regular peak against the degree of misalignment. The recorded values were fitted using the exponential regression as it offered the best statistical RMSE and Adjusted R-Square Values [47], which should be close to 0 and 1 respectively for the best statistical fit. A value closer to 1 for adjusted R-square shows that the regression model can be used for prediction with good accuracy [47]. The RMSE value closer to zero indicates that the value predicted by the regression model is very close to the actual value [47]. This procedure was repeated for all types of lateral and angular misalignments and the results are discussed below. As hypothesized before, increasing radial, axial and yaw misalignment would cause the signal RMS to decline because of the decrease in metal surface contact area. This trend was obtained in the total signal RMS, the shaft speed frequency and the GMF of vibration and the airborne sound signals under radial, axial and yaw misalignments as shown in Figs. 12-13 (a, b, and c respectively).

Pitch misalignments test was performed in the range of  $0^\circ$  to  $0.2^\circ$ . It was explained above that pitch misalignment could cause the loss of contact across the face width and this causes more face edge striking (gear damage) which results in more noise. Pitch misalignment also puts more axial loads on bearings and is treated as the most unsafe misalignment. This was reflected in an increase in RMS levels as pitch misalignments was increased and is shown in Figs. 12-13 (d). A creaking noise was also observed from the bearings in experiments where misalignments were greater than  $0.2^\circ$ . Hence tests were not performed above than this range. The trends for the total RMS of the signal, the shaft speed and the GMF are shown in Figs. 12-13 (d) for pitch misalignment tests.

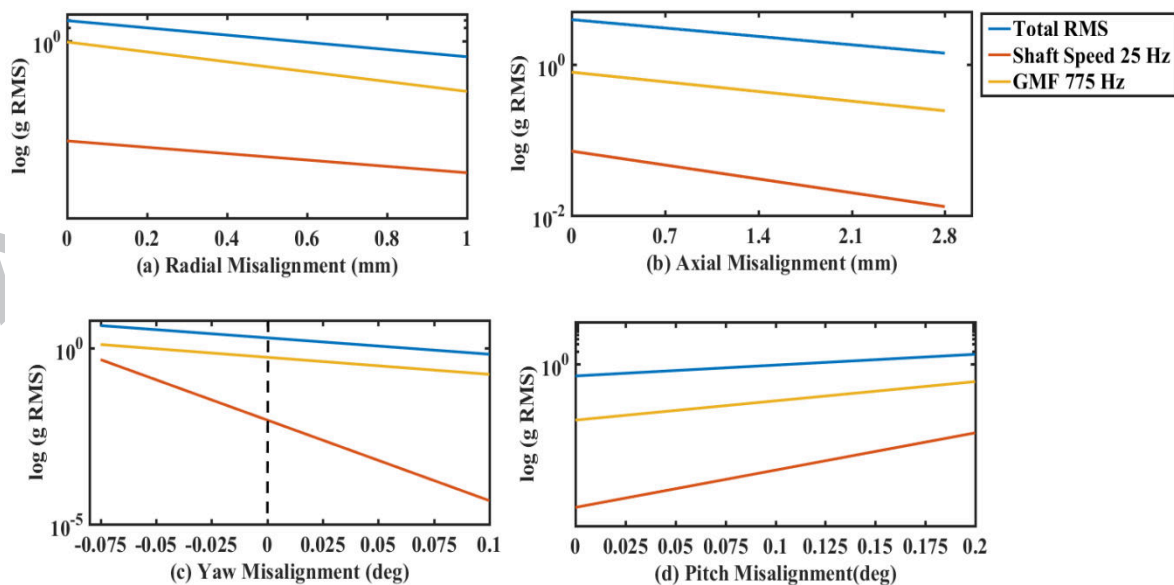


Fig. 12 Vibration Signal RMS trends for misalignment tests

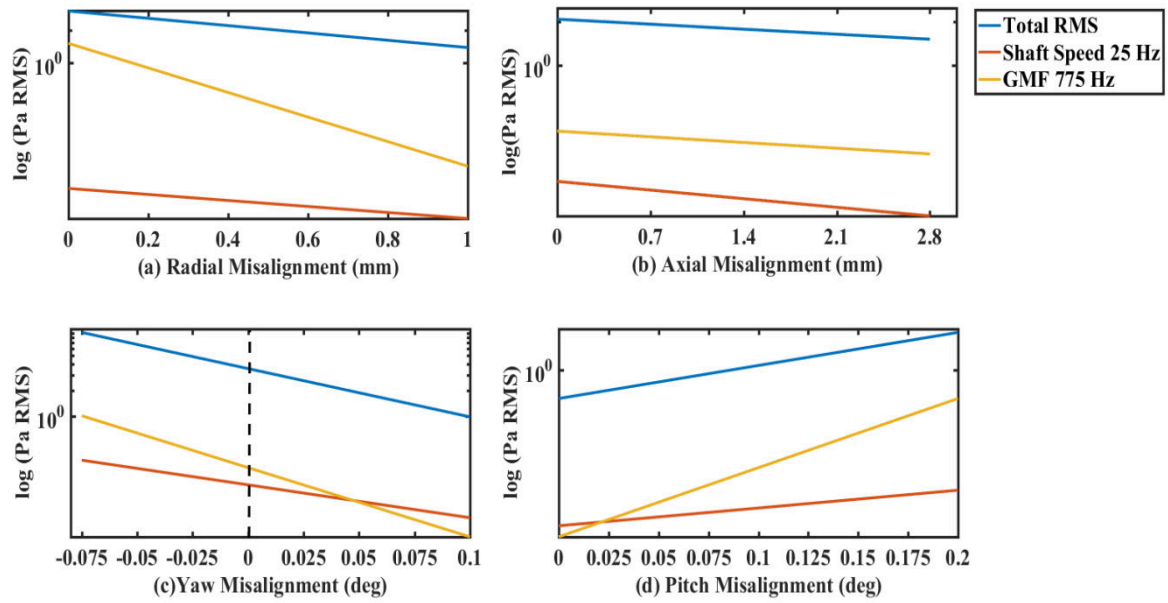


Fig. 13 Noise Signal RMS trends for misalignment tests

The RMSE and the Adjusted R-square values for all the curves shown in Figs. 11-12 used the exponential regression models and their values are shown below in Table 6.

Table 6 Goodness of fit statistics values for signal components

Misalignment	Signal	RMS Component	RMSE	Adjusted R-square
Radial	Vibration	Total RMS	0.3648	0.8483
		25Hz	0.000503	0.9213
		775 Hz	0.1336	0.8608
	Airborne sound	Total RMS	0.22383	0.87458
		25Hz	0.00158	0.97208
		775 Hz	0.15918	0.9256
Axial	Vibration	Total RMS	0.6118	0.7979
		25Hz	0.006588	0.9276
		775 Hz	0.08109	0.8815
	Airborne sound	Total RMS	0.1286	0.7844
		25Hz	0.1653	0.8107
		775 Hz	0.02762	0.8858
Yaw	Vibration	Total RMS	0.2198	0.9754
		25Hz	0.008211	0.9943
		775 Hz	0.08683	0.9472
	Airborne sound	Total RMS	0.21981	0.98266
		25Hz	0.01981	0.60432
		775 Hz	0.01636	0.99884
Pitch	Vibration	Total RMS	0.08123	0.9713
		25Hz	0.000913	0.9875
		775 Hz	0.03606	0.913
	Airborne sound	Total RMS	0.07746	0.9732
		25Hz	0.01391	0.7192
		775 Hz	0.05866	0.9387

The Kurtosis represents how peaked or flat the frequency amplitude distribution is. It is proposed that for radial, axial and yaw misalignments, Kurtosis should decrease with increasing misalignments. The peakedness of the amplitude distribution represents the intensity of gear meshing energy. As the misalignment is increased, the number of surface asperities coming into contact on gears decreases reducing the meshing energy intensity. This will cause the amplitude distribution to become flatter, hence reducing the Kurtosis value. This trend in Kurtosis for radial, axial and yaw misalignments is displayed in Figs. 14-15 (a, b and c respectively) for vibration and airborne sound signals. Exponential regression was used for curve fitting as it gave the best RMSE and Adjusted R-Square Values as given in Table 7.

As proposed for RMS, the vibration energy levels increases when gears wear under pitch misalignment. The increased edge striking causes increased gear damage (edge wear), which would cause Kurtosis to increase as well. This is displayed in Figs. 14-15, (d) for vibration and airborne sound signals under pitch misalignment.

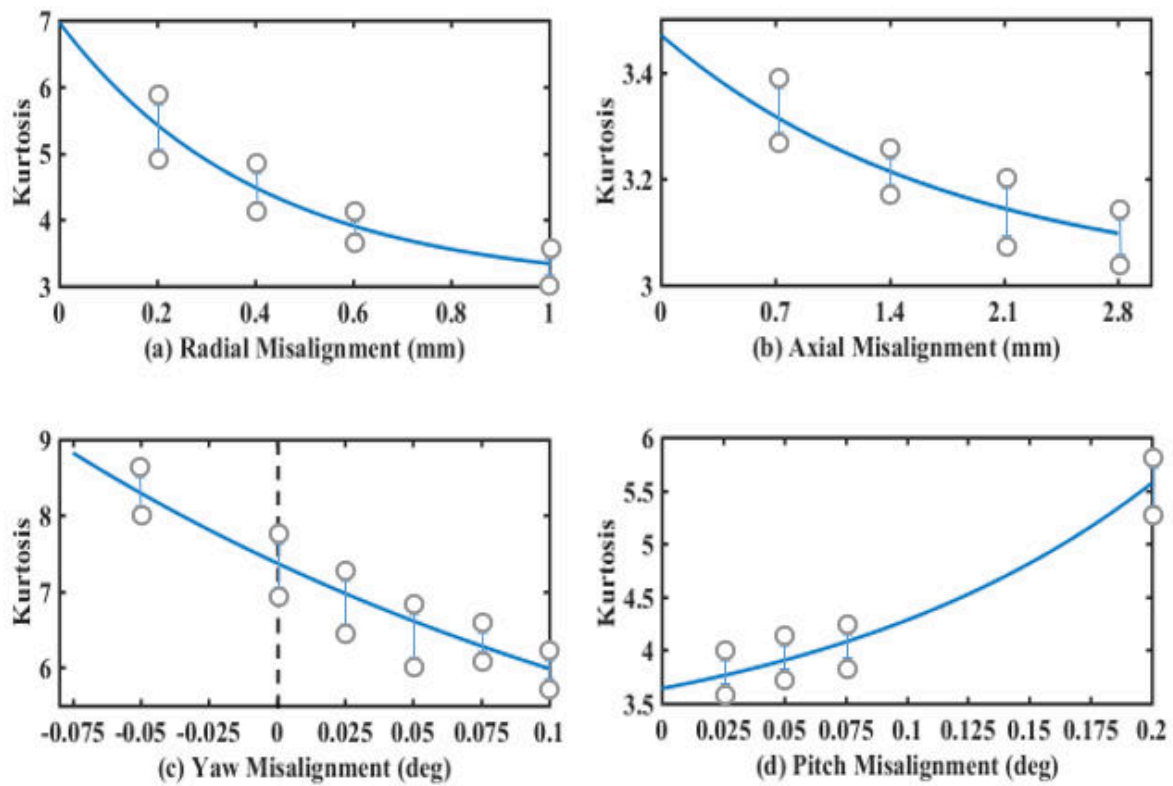


Fig.14 Vibration Signal Kurtosis for misalignment tests

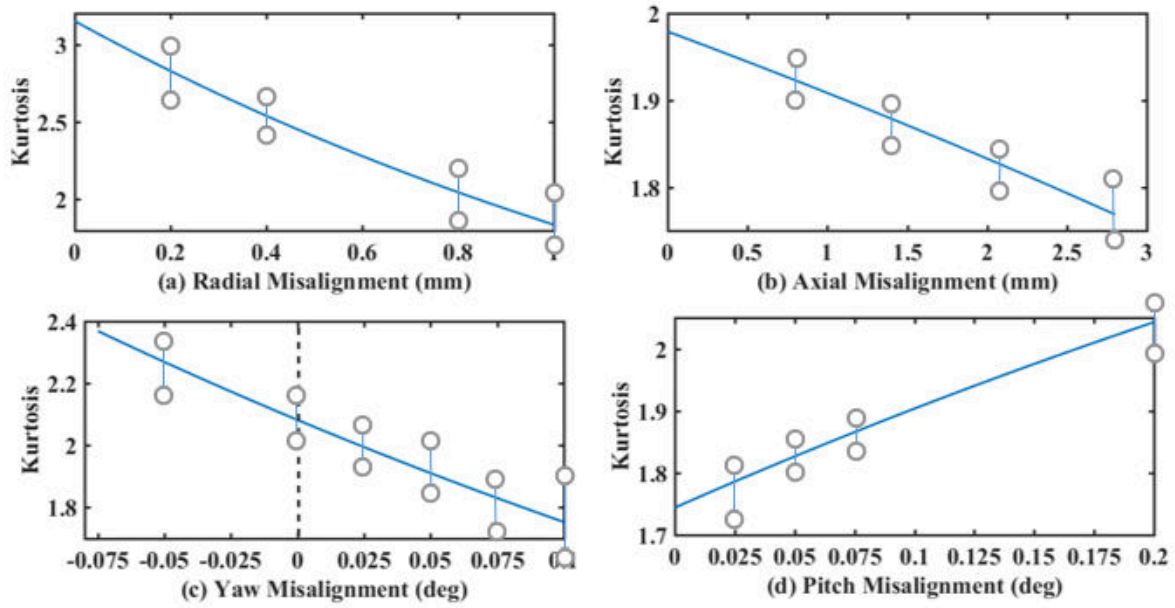


Fig. 15 Airborne sound Signal Kurtosis for misalignment tests

Table 7 RMSE and Adjusted R-Square for Curve Fitting Kurtosis

Misalignment	Signal	Adjusted R-Square	RMSE
Radial	Vibration	0.8135	0.6887
	Airborne sound	0.9587	0.08832
Axial	Vibration	0.3938	0.2049
	Airborne sound	0.8519	0.04451
Yaw	Vibration	0.9464	0.2379
	Airborne sound	0.9296	0.03776
Pitch	Vibration	0.8003	0.3611
	Airborne sound	0.7039	0.07154

Skewness of the vibration and the airborne sound signals indicate the symmetric characteristics of amplitude histograms. A time series with many small values and few large values is positively skewed. The spiky nature with few large values of time domain signal is indicative of higher skewness and higher vibration levels as shown in a typical aligned case in Fig. 16.

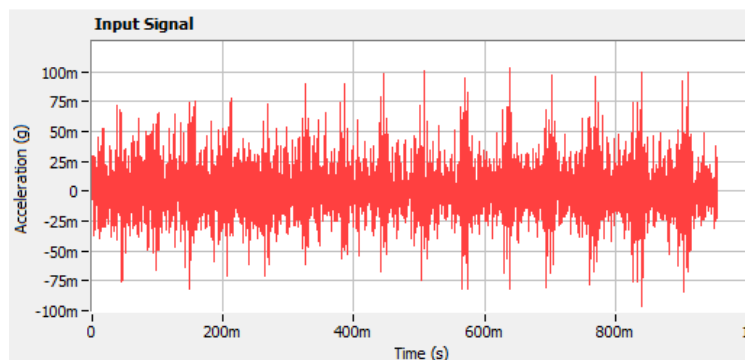


Fig. 16 Time domain vibration signal under aligned condition

The skewness value is proposed to drop with increasing radial, axial and yaw misalignment as the spiky nature (few large values in the time domain signal) decreases (i.e. number of large values relative to overall signal, increases), and amplitude levels drop as well. This is shown in Figs. 17-18 (a, b, c respectively) for vibration and noise signals.

For pitch misalignment, the skewness is proposed to increase with increasing misalignment. This will happen because the vibration amplitude levels will increase and there will be fewer large peaks in time domain signal as a result of more gearbox damage (edge wear). This is shown in Figs. 17-18 (d) for both vibration and airborne sound signals.

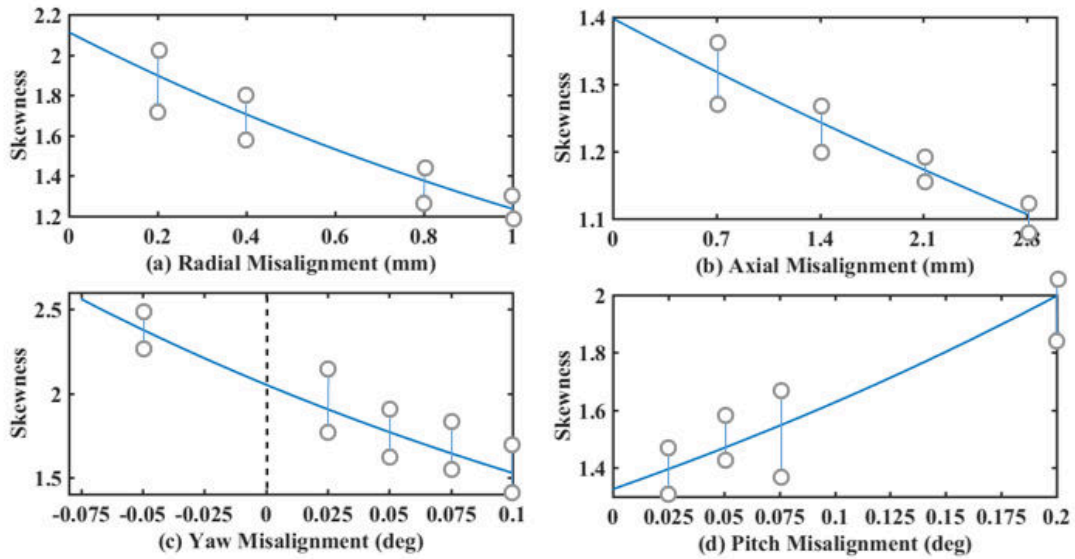


Fig. 17 Vibration Signal Skewness for misaligned tests

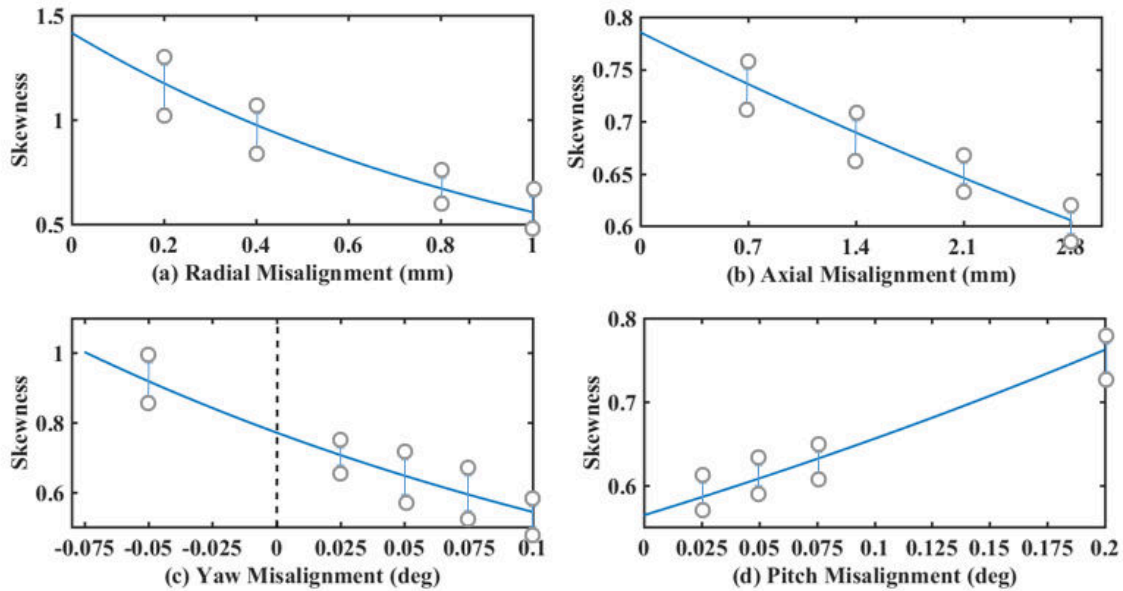


Fig. 18 Airborne sound Signal Skewness for all misaligned tests

The curve fitting exponential regression values for skewness are shown in Table 8.

Table 8 Regression Curve Fitting Values for Skewness

Misalignment	Signal	Adjusted R-Square	RMSE
Radial	Vibration	0.7789	0.1691
	Airborne sound	0.9836	0.03542
Axial	Vibration	0.8519	0.04451
	Airborne sound	0.4547	0.06696
Yaw	Vibration	0.8485	0.1613
	Airborne sound	0.9213	0.0314
Pitch	Vibration	0.9128	0.07936
	Airborne sound	0.6398	0.05441

Consistency in results was observed with RMS, Kurtosis and Skewness analysis for all the misalignments tests carried out. But, RMS is used for further discussion, from this point onwards to make regression models for misalignment prediction purposes. It indicates the variation in the overall energy content of the signals, with the change in misalignment, and hence seems a better indicator.

## 6. Discussion

The principle cause of the gear noise in the meshing process is the impact and the separation of the gear teeth that comes into contact. In the results mentioned above it was observed that the radial, the axial and the yaw misalignments caused a loss in the contact area in the meshing region. This reduced the number of surface asperities coming into contact and hence reduced the overall energy of the vibration and the noise signals as reflected by the curves of the total RMS, the energies of the shaft speed and the gear meshing frequency. The pitch misalignment caused more contact at the edges of the face width and hence increased the vibration levels. This caused more edge wear/chipping and heavy loads on the bearings. This was reflected as an increase in the energy levels of the total RMS of the signals, the energies at the shaft speed and the GMF. The change in RMS under pitch misalignment was not due to the reduction in number of surface asperities coming into contact, but the intensity of edge strikes (gear damage). The hypothesis of the change in the RMS due to the change in the meshing area or the change in number of surface asperities coming into contact, did not stand for the pitch misalignment and hence expressed in degrees.

It was assumed that the principles would be the same for change in the RMS values of the gears of any type or size if subjected to misalignments. Therefore, the axial, the radial and the yaw misalignments can be characterized in terms of the relative change or loss in tooth contact area inside the meshing zone. The relationship between the two variables (i.e. change in RMS values and contact area) can be generalized for all types and sizes of the gears. This would allow the prediction of the percentage loss in contact area of the meshing teeth provided the percentage loss in signal RMS is known. For this purpose, the designed gears were imported into SolidWorks© and the area calculations for each misaligned case of the axial, the radial and the yaw misalignments were performed and discussed below. The gear tooth face was a curved profile so projections were used to calculate the approximate area by assuming the tooth face as straight surfaces. The conditions for each misalignment were simulated in SolidWorks© and misalignments were replicated as they were carried out on the test rig. The replication model steps are shown in Figs. 19. The process was started by positioning the gears in the required conditions.

Once the pinion and gear were positioned in required alignment, planes and split lines were made to confine the approximate contact area as shown in Fig. 19 (a). This method created the split line on the tooth face of the adjacent gear and showed the line where the teeth would come in contact. The split lines were created on the tooth faces of both the driving and the driven gears. In the next step, straight

lines were created in between the split lines and the adjacent tooth edge to denote the corners of the contact area as shown in Fig. 19 (b).

A small portion of the split line was noticed to be out of contact with tooth edge as shown in Fig. 19 (c) which was rejected. In the final step, the corners were simply connected to obtain the contact area shown in Fig 19 (d). SolidWorks© *Measure* tool was used to calculate the contact area. The highest possible accuracy was used to obtain the precise values. These areas were the closest approximation to the actual contact area.

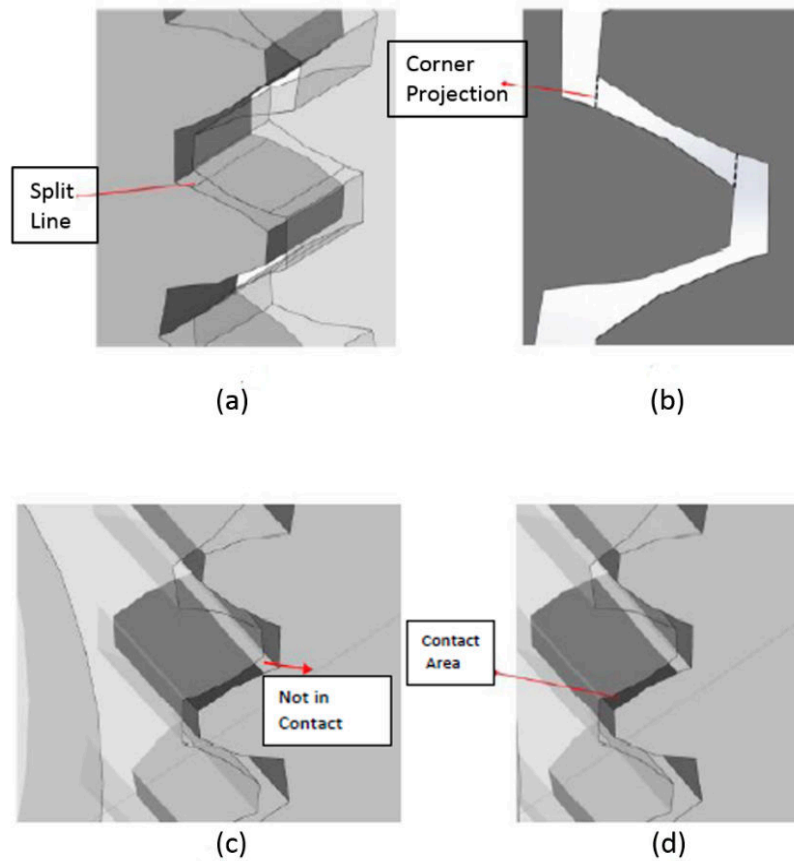


Fig. 19 Steps for Area Calculation in SolidWorks©

After the calculations of areas, the percentage loss in area for each misalignment case was calculated by using Equation 6:

$$\%Area\ loss = \frac{Area_{aligned} - Area_{misaligned}}{Area_{aligned}} \times 100 \quad (6)$$

The % loss in meshing area calculations are listed in Table 9.

Table 9 Area loss Calculation

Misalignment								
	Degree (°)	0°	0.025°	0.05°	0.075°	0.1°	-0.025°	-0.075°
Yaw	Area (mm <sup>2</sup> )	118.68	110.21	102.05	93.8	85.5	126.41	134.27
	% loss	0	7.13	14.009	20.88	27.95	-6.51	-13.13

Axial	Degree (mm)	0	0.7	1.4	2.1	2.8	
	Area (mm <sup>2</sup> )	118.68	115.068	111.45	107.84	104.23	
	% loss	0	3.04	6.08	9.13	12.17	
Radial	Degree (mm)	0	0.2	0.4	0.6	0.8	1
	Area (mm <sup>2</sup> )	118.68	114.08	109.48	104.88	100.28	95.68
	% loss	0	3.87	7.75	11.62	15.5	19.37

The aligned condition RMS value for each misalignment type was characterized as the baseline value. The percentage loss in signal RMS for each succeeding misalignment test was calculated in difference with this as given in Equation 7:

$$\% \text{loss in RMS} = \frac{RMS_{aligned} - RMS_{misaligned}}{RMS_{aligned}} \times 100 \quad (7)$$

The relative change in the energy content of the vibration and the air-borne sound signals with the relative change in the tooth meshing area is now discussed for radial, axial and yaw misalignment in Figs. 20-21 (a, b, c respectively).

The highly unsafe and severe characteristic of pitch misalignment is shown in Figs. 20-21 (d) in which a rise of about 8 times is observed in RMS energy of GMF, and 2 times in total signal RMS of vibration and airborne sound signals when exposed to up to 0.2° of pitch misalignment

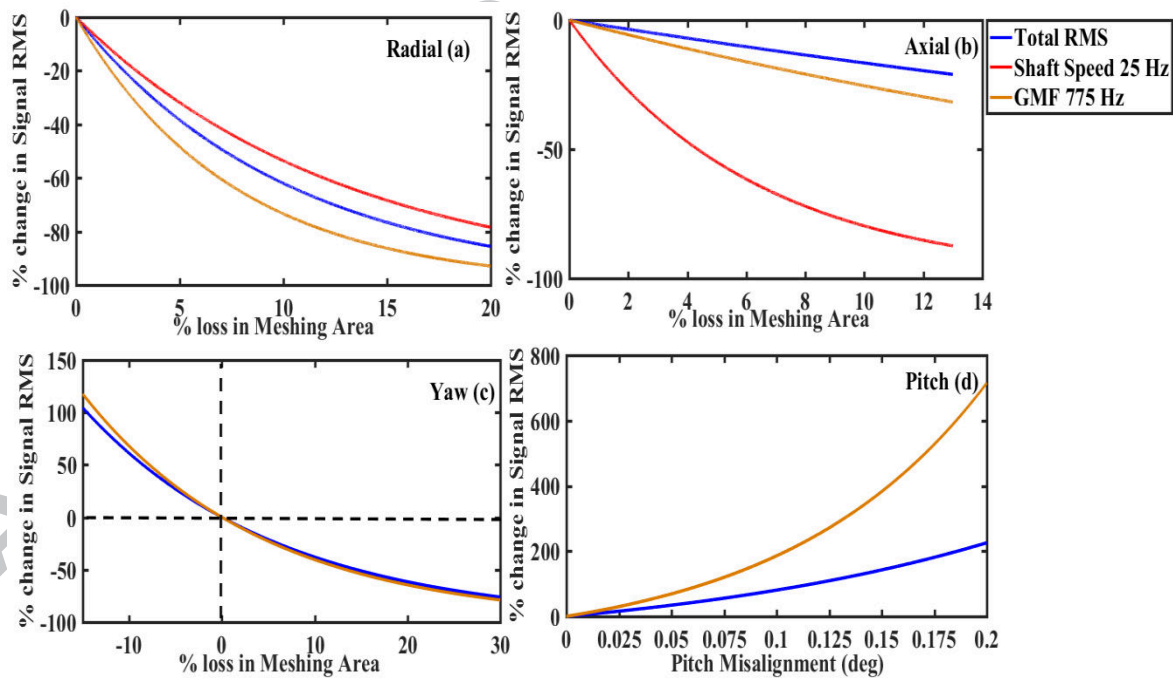


Fig. 20 Regression based Misalignment Prediction models for Vibration Signals

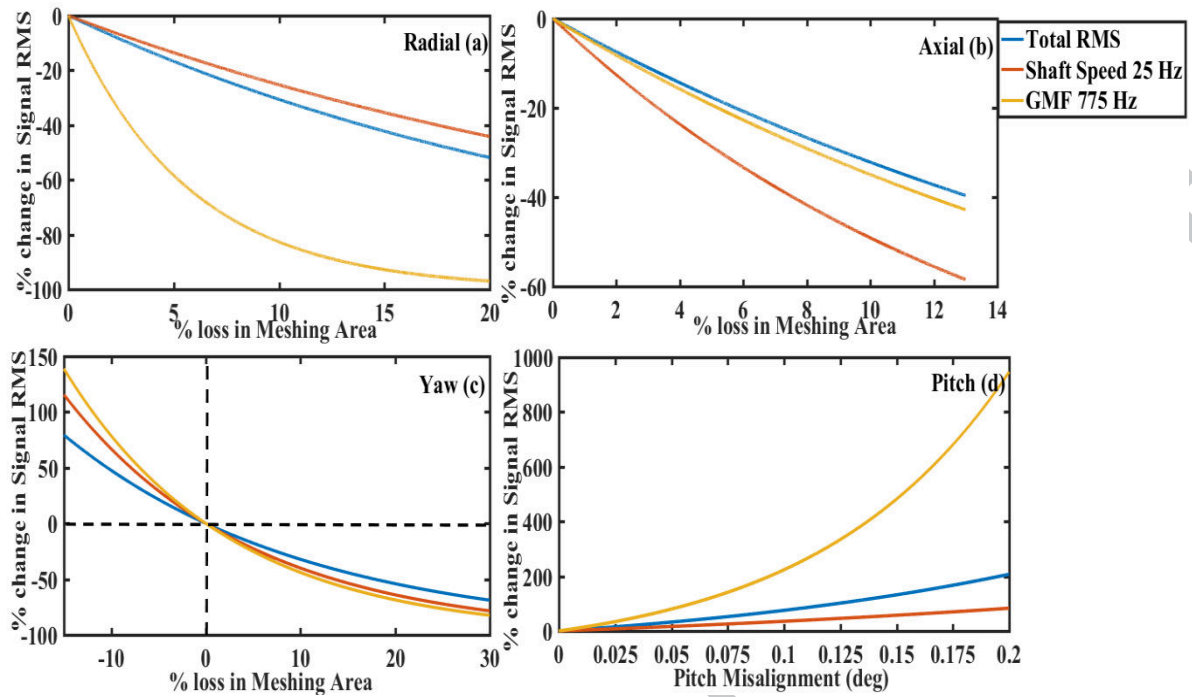


Fig. 21 Regression based Misalignment Prediction models for Airborne sound signals

These relation graphs between RMS change and misalignment tests were then validated with following additional misalignment tests carried out on the gear testing rig, and errors are specified in Table 10. The validation tests were repeated 3 times each. The signal RMS values were taken from SignalExpress™ and compared with values from the regression models developed above. The percentage error was calculated as given in Equation 8.

$$\% \text{Predicition Error} = \frac{RMS_{\text{observed}} - RMS_{\text{predicted}}}{RMS_{\text{observed}}} \times 100 \quad (8)$$

Table 10 Validation Readings for the Regression models with errors specified.

Misalignment	Signal	FFT Component	Misalignment used for validation	Observed RMS of validation point from experiment	Predicted RMS of validation point from regression	Prediction Error
Radial	Vibration	Total RMS	0.3mm	1.6742	1.624	2.9
		25Hz		0.0038	0.0033	13.1
		775 Hz		0.462	0.4345	5.9
	Airborne sound	Total RMS		2.5948	2.3619	8.9
		25Hz		0.0622	0.0596	4.1
		775 Hz		0.5923	0.696	-17.5
	Vibration	Total RMS	0.8mm	0.6420	0.6354	1.0
		25Hz		0.0020	0.0016	20
		775 Hz		0.1430	0.1204	15.8

	Airborne sound	Total RMS		1.8010	1.6096	10.6
		25Hz		0.0420	0.0435	-3.5
		775 Hz		0.1610	0.1922	-19.3
Yaw	Vibration	Total RMS		3.1998	3.0594	4.38
		25Hz		0.0030	0.0041	-36.6
		775 Hz		1.1400	0.8690	23.7
	Airborne sound	Total RMS	-0.025deg	5.1740	4.8330	6.5
		25Hz		0.1820	0.2060	-13.1
		775 Hz		0.4180	0.4109	1.6
	Vibration	Total RMS		1.054	1.008	4.3
		25Hz		0.000422	0.00038	9.9
		775 Hz		0.2913	0.2761	5.2
	Airborne sound	Total RMS	+0.06deg	1.7892	1.6445	8.0
		25Hz		0.08862	0.0988	-11.4
		775 Hz		0.09678	0.0876	9.4
Pitch	Vibration	Total RMS		0.9856	0.9553	3.0
		25Hz		0.003614	0.00312	13.6
		775 Hz		0.1459	0.1362	6.6
	Airborne sound	Total RMS	0.1 deg	1.18	1.0747	8.9
		25Hz		0.08902	0.0955	-7.2
		775 Hz		0.168	0.1895	-12.7
	Vibration	Total RMS		1.29521	1.28316	0.9
		25Hz		0.002	0.000863	56.8
		775 Hz		0.36	0.227	36.9
	Airborne sound	Total RMS	0.15 deg	1.31457	1.4227	-8.2
		25Hz		0.118	0.1111	5.8
		775 Hz		0.23	0.33	-43.4
Axial	Vibration	Total RMS		0.769986	0.7659	0.5
		25Hz		0.0029	0.00267	7.9
		775 Hz		0.18	0.1828	-1.5
	Airborne sound	Total RMS	2.1 mm	1.74431	1.4793	15.1
		25Hz		0.077	0.0830	-7.7
		775 Hz		0.413	0.2398	41.9
	Vibration	Total RMS	3.5 mm	0.7326	0.6771	7.5

Airborne sound	25Hz	0.000221 24	0.00015	32.2
	775 Hz	0.1248	0.1529	-22.5
	Total RMS	1.2126	1.3	-7.2
	25Hz	0.06724	0.0550	18.2
	775 Hz	0.1723	0.164	4.8

It can be noted from [Table 9](#), the total RMS values predicted by the regression models are very close to the actual values for all misalignment types. The largest error for the total RMS (15.2%) was observed in the airborne sound signal of axial misalignment. This could be explained by the external noise coming from the unwanted sources in the testing area. The high prediction errors occurring in other components of the FFT (like shaft speed frequency and GMF). This was because of the fact that the shaft misalignments could distribute the energy of the source speed running frequency into its harmonics. This could result an increase in the amplitudes of 2X, 3X and 4X shaft speeds. The noise bed in FFT would not be reduced by the same proportion as we used 250-times average in each test. Further, the energy of the GMF could also leak into its sidebands and the proportion that leak into the sidebands may be unique for each misalignment type. Hence the change in total RMS content of the signal could be a better measure for type of misalignment as, compared to the energy of the shaft speed or the GMF.

One more source of error could be the fact that the base table is not perfectly rigid, and since it has the highest mass amongst the rig components, it may have some vibrating energy when the rig is running, contributing to the signal noise. Bolting the base table to the floor and adding dampers can help reduce the error. Vibrations that result from varying mesh stiffness, bearing stiffness, variation in motor torque and dynamic misalignments are other sources of error. Using a voltage stabilizer could have reduced the voltage fluctuations, minimizing the variation in motor torque. Moreover, the fact that there could be machining tolerance errors, manufacturing defects, involute and spacing errors in gear geometry cannot be over ruled. The rig assembly could be dismantled and reassembled between each misalignment test to remove the effects of the configuration errors. But even in real world machineries, the system is not dismantled when small faults are repaired, hence errors in our models due to configuration closely approximate the machines in practical world. Above all, the alignment of gears to perfection is never possible and error due to this will always be present.

The parametric equations for the Total RMS curves based misalignment prediction models shown in [Figs. 20-21](#), have been inversed and are given in [Table 10](#). The type of misalignment for any given faulty signal would be identified by examining which of the trends developed in [Figs. 12-13](#) it closely follows. This would be done by computing the absolute change in RMS using the provided relative percentage change in RMS from baseline aligned to any misaligned condition for any faulty case. This difference can then be examined amongst all graphs in [Figs 12-13](#) and the curve it closely matches with would identify the type of misalignment. The equations in [Table 11](#) can then be used to compute the degree of misalignment in terms of the relative change in meshing area (variable Y) (except for pitch misalignment for which case Y is the absolute pitch misalignment), given that the relative change in signal RMS (variable X) from baseline aligned condition to any misaligned condition is provided. The advantage of this proposed framework is: the type or degree of shaft misalignment in any gearbox could be approximated (within the range of misalignments studied in this work) in terms of relative percentage change from aligned to any misaligned condition, irrespective of the gears' dimensions.

Table 11 Total RMS curves parametric equations for the misalignment diagnostic prediction models

Misalignment	Signal	Total RMS Parametric Model
--------------	--------	----------------------------

Radial	Vibration	$Y=-10.32*\ln(0.01*X+1)$
	Airborne sound	$Y=-27.32*\ln(0.01*X+1)$
Axial	Vibration	$Y=-12.561*\ln(0.01*X+1)$
	Airborne sound	$Y=-9.425*\ln(0.01*X+1)$
Yaw	Vibration	$Y=-20.97*\ln(0.01*X+1)$
	Airborne sound	$Y=-25.68*\ln(0.01*X+1)$
Pitch	Vibration	$Y=0.1694*\ln(0.01*X+1)$
	Airborne sound	$Y=0.1782*\ln(0.01*X+1)$

## 7. Conclusion and Future Work

The results show the efficacy of using the regression models developed in this research, for predicting the type and degree of misalignment for gears used in this research when the relative change in RMS from baseline condition is known. It is proposed to use only the relative change in total signal RMS for the prediction purposes as it offers the least error for all misalignment types. The misalignments prediction framework developed could be used for any gear in terms of the relative loss in the teeth meshing area, with the specified error. This study can help to improve the existing HUMS systems in detection of the dynamic misalignment problems.

The regression models can be improved with more experimentations for each type of misalignment. Gearbox condition health indicators like Crest Factor and Energy Ratio can also be studied to investigate the effect of different misalignment on these statistical tools. The research was limited to the time domain analysis in this research work, but can also be extended to frequency domain, time-frequency domain and cepstrum analysis. The presented work considered one type of misalignment in each of the performed experiments, which would not always be the real scenario. The tests were also limited to constant load and a fixed running speed. In the real world, dynamic forces can cause a combination of angular and lateral misalignments, hence combined misalignment tests under variable loads and different running speeds will be carried out in near future which will significantly improve the impact of the presented work. The proposed method can be applied to misalignment diagnosis in other types of gears including worm, bevel and helical gears to further support the hypothesis. This warrants modifications to the test rig which requires considerable time, effort and funding. Gear rig modification and misalignment tests for other types of gears will be carried out in the near future.

## References:

- [1] D. Learmount, "Rotary woes," *Flight Int.*, vol. 157, no. 4725, p. 34, 2000.
- [2] A. A. I. Branch, "2/2011 G-REDL," 2011.
- [3] A. Safety, "Security Program, the Helicopter Accident Analysis Team," Final Rep. Helicopter Accid. Anal. Team, 1998.
- [4] M. Lebold, K. McClintic, R. Campbell, C. Byington, and K. Maynard, "Review of vibration analysis methods for gearbox diagnostics and prognostics," presented at the Proceedings of the 54th meeting of the society for machinery failure prevention technology, 2000, vol. 634, p. 16.
- [5] R. Bajric, D. Spreicic, and N. Zuber, "Review of vibration signal processing techniques towards gear pairs damage identification," *Int. J. Eng. Technol.*, vol. 11, no. 4, pp. 124–128, 2011.
- [6] M. Nie and L. Wang, "Review of condition monitoring and fault diagnosis technologies for wind turbine gearbox," *Procedia Cirp*, vol. 11, pp. 287–290, 2013.

- [7] V. Giurgiutiu, A. Cuc, and P. Goodman, "Review of vibration-based helicopters health and usage monitoring methods," South Carolina Univ Columbia Dept Of Mechanical Engineering, 2001.
- [8] A. A. I. Branch, "Report on the accident to Aerospatiale (Eurocopter) AS332 L2 Super Puma, registration G-REDL 11 nm NE of Peterhead, Scotland on 1 April 2009," EW, 2009.
- [9] J. E. Shigley, Shigley's mechanical engineering design. Tata McGraw-Hill Education, 2011.
- [10] R. Tharmakulasingam, "Transmission error in spur gears: Static and dynamic finite-element modeling and design optimization," 2010.
- [11] M. Åkerblom, Gear Noise and Vibration: A Literature Survey. 2001.
- [12] S. More, K. Ghadge, and S. Chillal, Design, analysis and measurement of transmission error, vol. 8. 2017.
- [13] R. Teja, T. Milind, R. C. Glover, and S. Sonawane, "Dynamic Analysis of Helical Gear Pair Due to TE and Shuttling Moment Excitations," SAE Technical Paper, 0148-7191, 2017.
- [14] J. Zhan, M. Fard, and R. Jazar, "A CAD-FEM-QSA integration technique for determining the time-varying meshing stiffness of gear pairs," Measurement, vol. 100, pp. 139–149, 2017.
- [15] R. V. Mulik, S. S. Ramdasi, and N. V. Marathe, "Dynamic Simulation of 6 Speed Gearbox of Tipper Application to Improve Gear Contact Life," SAE Technical Paper, 0148-7191, 2017.
- [16] R. Zhang and T. Wang, Experiment and Simulation Study on the Gear Tooth Modification of Helical Gear Pair based on Dynamic Performances, vol. 10. 2017.
- [17] A. Jammal, C. Gu, H. Wang, R. Li, Y. Song, and Y. K. Rong, "An experimental study on high speed helical gears misalignments and dynamic behavior under random loading," in 2016 7th International Conference on Mechanical and Aerospace Engineering (ICMAE), 2016, pp. 234–238.
- [18] O. J. Harris, P. P. Langlois, and G. Cooper, "Noise Reduction in an EV Hub Drive Using a Full Test and Simulation Methodology," Gear Technol., 2016.
- [19] C. H. Wink, "Gear Backlash Analysis of Unloaded Gear Pairs in Transmissions."
- [20] H. Ameen, "Effect of shaft misalignment on the stresses distribution of spur gears," Eng Tech J, vol. 28, pp. 1321–1339, 2010.
- [21] R. Jones, K. Mao, A. Phang, and B. Allen, "Effects of linear and angular misalignment on a spur gear pair," Insight-Non-Destr. Test. Cond. Monit., vol. 53, no. 8, pp. 420–425, 2011.
- [22] S. Prabhakaran, D. Balaji, and C. Joel, "Stress analysis and effect of misalignment in spur gear," Int. J. Appl. Eng. Res., vol. 9, no. 22, pp. 13061–13071, 2014.
- [23] M. Lias, T. Rao, M. Awang, and M. Khan, "The Stress Distribution of Gear Tooth Due to Axial Misalignment Condition," J. Appl. Sci., vol. 12, pp. 2404–2410, 2012.
- [24] R. G. Jones, "The mathematical modelling of gearbox vibration under applied lateral misalignment," 2012.
- [25] S.-Y. Ye and S.-J. Tsai, "A computerized method for loaded tooth contact analysis of high-contact-ratio spur gears with or without flank modification considering tip corner contact and shaft misalignment," Mech. Mach. Theory, vol. 97, pp. 190–214, 2016.
- [26] Zhu, J., Nostrand, T., Spiegel, C., & Morton, B. (2014). Survey of condition indicators for condition monitoring systems. In *Annual Conference of the Prognostics and Health Management Society* (Vol. 5, pp. 1-13).

- [27] J. J. Zakrajsek, "An investigation of gear mesh failure prediction techniques," NATIONAL AERONAUTICS AND SPACE ADMINISTRATION CLEVELAND OH LEWIS RESEARCH CENTER, 1989.
- [28] A. Ogundare, S. Ojolo, D. Mba, and F. Duan, "Review of fault detection techniques for health monitoring of helicopter gearbox," in *Advanced Technologies for Sustainable Systems*, Springer, 2017, pp. 125–135.
- [29] A. S. Sait and Y. I. Sharaf-Eldeen, "A review of gearbox condition monitoring based on vibration analysis techniques diagnostics and prognostics," in *Rotating Machinery, Structural Health Monitoring, Shock and Vibration*, Volume 5, Springer, 2011, pp. 307–324.
- [30] S. Shukla and V. K. Karma, "Fault Detection of Two Stage Spur Gearbox using Time Domain Technique: Effect of Tooth Breakage and Improper Chamfering," *IJISSET-Int. J. Innov. Sci. Eng. Technol.*, vol. 1, no. 4, pp. 184–189, 2014.
- [31] Y. Lei, J. Lin, M. J. Zuo, and Z. He, "Condition monitoring and fault diagnosis of planetary gearboxes: A review," *Measurement*, vol. 48, pp. 292–305, 2014.
- [32] Z. Chen and Y. Shao, "Dynamic simulation of spur gear with tooth root crack propagating along tooth width and crack depth," *Eng. Fail. Anal.*, vol. 18, no. 8, pp. 2149–2164, 2011.
- [33] D. Lin, M. Wiseman, D. Banjevic, and A. K. Jardine, "An approach to signal processing and condition-based maintenance for gearboxes subject to tooth failure," *Mech. Syst. Signal Process.*, vol. 18, no. 5, pp. 993–1007, 2004.
- [34] O. D. Mohammed, M. Rantatalo, and J.-O. Aidanpää, "Improving mesh stiffness calculation of cracked gears for the purpose of vibration-based fault analysis," *Eng. Fail. Anal.*, vol. 34, pp. 235–251, 2013.
- [35] N. Baydar and A. Ball, "Detection of gear failures via vibration and acoustic signals using wavelet transform," *Mech. Syst. Signal Process.*, vol. 17, no. 4, pp. 787–804, 2003.
- [36] Y. Qu, D. He, J. Yoon, B. Van Hecke, E. Bechhoefer, and J. Zhu, "Gearbox tooth cut fault diagnostics using acoustic emission and vibration sensors—A comparative study," *Sensors*, vol. 14, no. 1, pp. 1372–1393, 2014.
- [37] H. J. Decker, "Crack detection for aerospace quality spur gears," 2002.
- [38] E. Bechhoefer, Y. Qu, J. Zhu, and D. He, "Signal processing techniques to improve an acoustic emissions sensor," presented at the Annual Conference of the Prognostics and Health Management Society, 2013, vol. 4, pp. 1–8.
- [39] C. J. Li and J. Limmer, "Model-based condition index for tracking gear wear and fatigue damage," *Wear*, vol. 241, no. 1, pp. 26–32, 2000.
- [40] J. Igba, K. Alemzadeh, C. Durugbo, and E. T. Eiriksson, "Analysing RMS and peak values of vibration signals for condition monitoring of wind turbine gearboxes," *Renew. Energy*, vol. 91, pp. 90–106, Jun. 2016.
- [41] A. Bilošová and J. Biloš, "Vibration diagnostics," Ostrava Google Sch., 2012.
- [42] J.-C. Gu and S.-L. Yu, "Removal of DC offset in current and voltage signals using a novel Fourier filter algorithm," *IEEE Trans. Power Deliv.*, vol. 15, no. 1, pp. 73–79, 2000.
- [43] Graham, R. L., Knuth, D. E., Patashnik, O., & Liu, S. (1989). *Concrete mathematics: a foundation for computer science*. *Computers in Physics*, 3(5), 106-107.

- [44] Scott, D. W. (1979). On optimal and data-based histograms. *Biometrika*, 66(3), 605-610.
- [45] J. Mais, "Spectrum analysis: the key features of analyzing spectra," 2002.
- [46] V. Skrickij and M. Bogdevičius, "Vehicle gearbox dynamics: centre distance influence on mesh stiffness and spur gear dynamics," *Transport*, vol. 25, no. 3, pp. 278–286, 2010.
- [47] J. Rafiee and P. Tse, "Use of autocorrelation of wavelet coefficients for fault diagnosis," *Mech. Syst. Signal Process.*, vol. 23, no. 5, pp. 1554–1572, 2009

# Gear misalignment diagnosis using statistical features of vibration and airborne sound spectrums

Khan, Muhammad Ali

2019-05-31

Attribution-NonCommercial-NoDerivatives 4.0 International

---

Khan M, Shahid M, Ahmed S, et al., (2019) Gear misalignment diagnosis using statistical features of vibration and airborne sound spectrums. *Measurement*. Volume 145, October 2019, pp. 419-435

<https://doi.org/10.1016/j.measurement.2019.05.088>

*Downloaded from CERES Research Repository, Cranfield University*